Journal of Materials Chemistry B

ROYAL SOCIETY OF CHEMISTRY

PAPER

View Article Online
View Journal

Cite this: DOI: 10.1039/d6tb00654j

Chitosan with defined intrinsic viscosity enables physicochemical entrapment of microplastics under *in vitro* gastric conditions†

Claudio Casella, *[a] Santiago Ballaz,[b] Rafael Luque [cd] and Umberto Cornelli[e]

Microplastics (MPs) are increasingly detected in food and biological systems, raising concerns about their interaction with the gastrointestinal environment. Strategies capable of limiting their mobility and epithelial contact are therefore of growing interest. Here, we investigate the role of chitosan physicochemical properties in the entrapment of MPs under *in vitro* gastric conditions (pH = 3 and 37 °C). Using chitosan samples with a comparable degree of deacetylation (DDA) but different intrinsic viscosities, we identify a threshold behaviour governing MP capture. Only chitosan with intrinsic viscosity ≥90 cP (corresponding to 100 kDa and ≥310 nm contour length) forms semi-dilute entangled networks capable of effectively entrapping high-density polyethylene (HDPE), polyvinyl chloride (PVC) and polyethylene terephthalate (PET) MPs, achieving up to 87% topological entrapment. Lower-viscosity variants remain in a dilute regime and show negligible binding. Combined proton nuclear magnetic resonance (^{1}H-NMR), thermogravimetric analysis (TGA), and scanning electron microscopy (SEM) demonstrate that this transition arises from the polymer architecture rather than the surface charge, enabling multipoint interactions and topological confinement within a continuous polymer network. These findings establish intrinsic viscosity as a key design parameter for polymer-based interception of MPs at the biointerface. While the biological fate of the resulting aggregates requires further investigation, this study provides a physicochemical framework for understanding and engineering polymer–MP interactions under gastric conditions. These findings suggest a new material-based approach for reducing the bioavailability of MPs by dietary intervention.

Received 23rd March 2026,
Accepted 15th April 2026

DOI: 10.1039/d6tb00654j

rsc.li/materials-b

1. Introduction

Microplastics (MPs) have become ubiquitous contaminants throughout the food chain, being detected in drinking water, salt, seafood, honey, bottled beverages[1] and more recently in human blood and intestinal tissues.[2] Their small size allows prolonged gastric residence, close interaction with the epithelium and, in some cases, potential translocation.[3] Chronic exposure has been associated with oxidative stress, inflammation and possible contributions to metabolic and cardiovascular dysfunction, neurotoxicity, hormonal dysregulation, and cancer.[4] Despite rising concerns about contamination across the food chain, few methods exist for lowering the gastric bioavailability of MPs.[5]

Chitosan—a β-(1 → 4)-linked copolymer of D-glucosamine and *N*-acetyl-D-glucosamine—has long been used as a biocompatible dietary fibre with gel-forming and adsorption properties.[6–8] Prior work has suggested its ability to interact with hydrophobic substances,[9] including lipids[10] and certain MPs.[11] However, the physicochemical features governing chitosan binding to MPs remain poorly defined. Specifically, whether its ability to physically entrap plastic particles under physiologically relevant conditions[12] depends on viscosity, molecular weight (MW) or polymer length is uncertain.[13]

From the standpoint of materials chemistry, chain architecture, solution concentration regime, and intermolecular interactions all influence polymer–particle interactions in acidic media. Specifically, the ability of polymers to form continuous networks and to physically restrict particulate matter is known to be drastically altered by the transition from dilute to semi-dilute entangled regimes. Nevertheless, there is currently no quantitative framework that connects the physicochemical

[a] Department of Chemistry, University of Pavia, Viale Taramelli 12, 27100, Pavia, Lombardy, Italy. E-mail: claudio.casella01@universitadipavia.it
[b] Materials and Processes Research Group, Distance University of Madrid (UDIMA), Carretera de La Coruña, KM. 38500 – Vía de Servicio, no. 15, CP 28400, Collado Villalba, Madrid, Spain. E-mail: sballaz@gmail.com
[c] Universidad ECOTEC, Km 13.5 Samborondón, Samborondón EC092302, Ecuador. E-mail: rluque@ecotec.edu.ec
[d] National University of Science and Technology POLITEHNICA Bucharest, 1-7 Gh. Polizu str., Bucharest, Romania
[e] Department of Molecular Pharmacology and Therapeutics, School of Medicine, Loyola University, Chicago, IL 60660, USA. E-mail: ucornelli@gmail.com
† This article is dedicated to Alexander Santiago Casella Flores.

characteristics of chitosan to its capacity to trap MPs under physiologically appropriate circumstances. By carefully investigating the function of intrinsic viscosity as a chitosan chain architectural descriptor in determining MP entrapment under gastric simulation scenarios (pH 3, 37 °C), we solve this gap. Using samples of chitosan with a comparable degree of deacetylation (DDA) but distinct molecular weights and contour lengths, we identify a threshold behaviour at which polymer chains form entangled networks that effectively trap MPs (high-density polyethylene, HDPE; polyvinyl chloride, PVC; and polyethylene terephthalate, PET).[12,14,15] We establish a structure–property–function relationship between intrinsic viscosity and particle entrapment effectiveness by combining viscometry, proton nuclear magnetic resonance (^{1}H-NMR), thermogravimetric analysis (TGA), and scanning electron microscopy (SEM). Intrinsic viscosity is identified as a crucial design characteristic for engineering such systems, and this study provides a materials-level framework for comprehending polymer-mediated interactions with MPs at the bio-interface.

2. Materials and methods

2.1. Chitosan samples

Four varieties of chitosan, specifically Chito 1 to 4, with 85–90% degrees of deacetylation (DDA) and unique intrinsic viscosities, were analyzed. All chitosan samples (Chito 1, Chito 2, Chito 3 and Chito 4) were obtained from commercial sources and used as benchmarks. Chito 3 is the only chitosan derivative that originates completely from a 100% monotypic biomass of *Procambarus clarkii*, according to scientific data. The intrinsic viscosity was determined by Huggins and Kraemer plots.[16] Chito 1 and 2 were standard polyglucosamine mixes from different sources that had similar DDA (between 85% and 90%) and varying viscosities (Chitosan 1 from 10 to 40 centipoise (cP) and Chitosan 2 from 60 to 80 cP). Chito 3 was a 90% deacetylated pure medium weight chitosan (from 90 to 130 cP) extracted from *Procambarus clarkii.* Finally, Chito 4 with higher viscosity (from 250 to 450 cP) was obtained from crustacean shells.[17]

Table 1 summarizes the physicochemical characteristics of the investigated chitosan samples. The inherent viscosity (η) was measured using a Cannon–Fenske capillary viscometer (size 100) immersed in a precision thermostatic water bath at 25.0 ± 0.1 °C. To lessen the impact of polyelectrolytes, the samples were dissolved in a solvent mixture of 0.2 M NaCl (Sigma-Aldrich, Darmstadt, Germany) and 0.1 M acetic acid (Sigma-Aldrich, Darmstadt, Germany).

η values were derived by extrapolating the reduced and inherent viscosities to zero concentration using the Huggins and Kraemer equations.[16,18] The viscosity-average molecular weight was subsequently calculated using the Mark–Houwink–Sakurada equation (eqn (1)):

$$\eta = K \cdot M_v^a \quad (1)$$

where K and a are constants. $K = 1.81 \times 10^{-3}$ mL g^{-1}, $a = 0.93$.

These values were applied for the specific solvent/temperature conditions used. The polymer contour length was estimated based on the degree of polymerization and the length of a single glucosamine monomer (≈0.515 nm), assuming a linear polysaccharide backbone.[16,18] Additionally, every chitosan sample used in this investigation included a DDA >85%, which was supplied by the manufacturer and verified to guarantee a high cationic charge density at acidic pH. To guarantee statistical reproducibility, every measurement was taken in triplicate. Intrinsic viscosity (cP), MW (kDa) and polymer length (nm) showed strong correlation with binding capacity (Table 1).

Table 1 Main physicochemical properties of the analyzed chitosan samples (DDA > 85%)

Sample	Intrinsic viscosity (cP)	MW (kDa)	Length (nm)
Chito 1	≈20	≈50	≈150
Chito 2	≈64	≈75	≈230
Chito 3	≈112	≈112	≈460
Chito 4	≈250	≈150	≈960

2.2. Chitosan and MP blending mode

Each chitosan was dissolved at 0.8 g L^{-1} in one liter of bi-distilled filtered water (Whatman filter, 0.7 μm pore size, Whatman, VWR, USA) that had been heated to 37 °C and had a pH = 3 after adding 0.1 N of HCl (Sigma-Aldrich, Darmstadt, Germany). It was followed by the addition of 0.5, 1.0, 2.0, 5, 10, and 30 mg L^{-1} of MPs. HDPE, PVC, and PET MPs were generated by cryo-grinding commercial products and sieving to 100–500 μm. To guarantee environmental relevance, the MPs were generated using widely used commercial food-grade materials. More specifically, rigid bottle caps were mechanically ground to produce HDPE, while commercial food containers and mineral water bottles were the origins of PVC and PET. These materials were identified as exemplary sources of secondary MP contamination in human food. Prior to processing, all plastic products were cryo-ground and sieved to the desired fraction of 100–500 μm as previously mentioned after being carefully cleaned with deionized water and ethanol (Sigma-Aldrich, Darmstadt, Germany) to eliminate organic residues.

To guarantee a well-defined size distribution, the MPs were produced by cryo-grinding and subsequent physical fractionation. The material was filtered and the 100–500 μm fraction separated using a stainless-steel sieving module with overlapping 500, 250 and 100 μm sieves (CISA Sieving Technologies, Barcelona, Spain). The MPs recovered using glass fibre filters (0.7 μm pore size, Whatman, Florham Park, NJ, USA) were methodically evaluated to ensure that the particles stayed within the specified range. A semi-automatic stereomicroscope (Leica M205FA, Leica Microsystems CMS GmbH, Wetzlar, Germany) and a high-resolution digital color camera (Leica DFC310FX; 1.4 Mpixel, CCD) were used to validate the MP size and morphology. The Confocal UniOvi ImageJ program (Version 1.54p) was used to measure the MP fragment and fibre diameters accurately. By verifying that the experimental fraction was contained within the designated 100–500 μm range, this thorough characterization avoided the possibility of larger aggregates or substantial amounts of sub-micrometer detritus that could have impacted the binding quantification.

Beakers with the mix were then submerged in a bath at 37 °C and swirled for 60 min at 30 rpm. The sedimentation process was then aided by a 1 h rest interval, after which the supernatant was gathered and filtered through glass microfibre filters (0.7 μm pore, Whatman). To prevent artificial aggregation or compaction resulting from external forces such as centrifugation, a sedimentation period of one hour was chosen to allow chitosan–MP aggregates to spontaneously settle through gravity. This time interval was empirically found to be appropriate to produce a distinct phase separation between bound and unbound fractions, while maintaining consistency with physiologically acceptable stomach residence stages. While longer resting times did not considerably improve aggregate recovery, shorter periods led to incomplete sediment progression. In addition, the quantity of sediment that accumulated at the test's beaker bottom was also collected.

To identify the physicochemical interactions between chitosan and MPs, the method for replicating stomach conditions was adjusted using well-established *in vitro* static digestion models. Although the basic parameters—such as a temperature of 37 °C and a sustained stomach pH of 3.0—align with established physiological benchmarks, the experimental protocol was modified to take into consideration the specific challenges associated with MP recovery. To avoid inorganic interaction with the polymer's surface-active functional groups, a simpler electrolyte-free matrix was developed.[6,9,10]

Briefly, MPs were suspended in the chitosan acidic solution under constant stirring (30 rpm) to ensure a homogeneous distribution. The system was then subjected to simulated gastric conditions, where the transition from a stable suspension to a polymeric–MP aggregate was monitored as a function of the chitosan molecular weight.[6,9,10]

Samples were stored in glass Petri dishes, where MP–chitosan hydrogels were allowed to fully dry at room temperature before being examined. Experiments were conducted in triplicate. The aim of the study was strictly limited to MPs in the 100–500 μm size range based on the cryo-grinding and sieving parameters.

2.3. ^{1}H-NMR spectra

A 400 MHz spectrometer (Bruker, Ettlingen, Germany) was used to record the ^{1}H-NMR spectra, in accordance with nuclear magnetic resonance principles. At room temperature, chitosan samples (15 mg) were dissolved in 700 μL D_2O acidified with 15 μL CD_3COOD; 16 scans were carried out for every spectral profile. Chemical shifts (δ) are reported in ppm relative to residual solvent peaks as internal standards. Signal multiplicities are indicated as s (singlet), d (doublet), t (triplet), q (quartet), or m (multiplet), and coupling constants (J) are given in Hz. The integral of the methyl signal of the *N*-acetylglucosamine units ($\delta \approx 2.0$ ppm) in relation to the signals of the glucopyranose ring protons (δ = 3.1–4.0 ppm) was used to compute the DDA.

2.4. TGA

A TGA/DSC (Mettler Toledo, Schwerzenbach, Switzerland) system was employed to carry out thermogravimetric analysis (TGA) in order to evaluate the chitosans' thermal stability and degradation behaviour. Both nitrogen and air atmospheres were employed for the measurements, which used a continuous heating rate from room temperature to higher temperatures. To guarantee accuracy and repeatability, the equipment was calibrated in accordance with the manufacturer's suggested methods prior to analysis. Standard alumina crucibles were filled with samples of controlled mass, and the mass loss was continually monitored as a function of temperature. The specialized Mettler Toledo software was used to evaluate the obtained thermograms in order to identify specific thermal transitions and decomposition phases. In order to maintain the required setting, analyses were often carried out throughout a temperature range of roughly 25–800 °C at a heating rate of 10 °C min^{-1} under controlled gas flow.

2.5. SEM imaging

A Hitachi EOL-6610LV SEM with X-ray microanalysis evaluated morphological interactions of the filtered hydrogels or films made of MPs and chitosan across 45 quadrants per condition. The SEM was completely automated, operated on a PC, and automatically saved micrograph images in the BMP, TIFF, or JPG formats. Analysis of the spatial distribution of the polymeric clusters and the effective diameter of the chitosan–MP aggregates was performed using ImageJ software to quantify the entrapment architecture (Confocal UniOvi ImageJ, LAS V4.0 Leica Application Suite, Version 4.0.0, Leica Microsystems CMS GmbH, Germany (https://imagej.net/nih-image/)). SEM images underwent semi-quantitative image analysis using ImageJ software in addition to qualitative evaluation. In particular, the spatial distribution of polymer networks, cluster density (measured as the number of contact events per field), and effective diameter of chitosan–MP aggregates were measured across $\geq$45 fields per condition. To provide statistical robustness, these parameters were averaged over trials. These measures allowed for a consistent comparative evaluation of structural organization across various chitosan viscosities, even though absolute surface coverage was not measured. By assigning typical ranges of events for each field, cluster density values were obtained from the categorical SEM scoring system (Table 3), allowing for semi-quantitative representation of geographic distribution trends.

2.6. Stereomicroscopy and quantitative entrapment

A semi-automated stereomicroscope (Leica M205FA, Leica Microsystems CMS GmbH, Germany) equipped with a high-resolution digital colour camera (Leica DFC310FX; 1.4 Mpixel, CCD; zoom from 7.85 to 161×) was used to inspect the formation of MP–Chito hydrogel aggregates. Colour-based segmentation of MPs *versus* chitosan binding images (% binding) were qualitatively scored as follows: 0 = no binding; 1 = moderate binding (10–20 events per quadrant): and 2 = extensive binding (>20 events). Experiments were run in triplicate. An 'event' refers to a distinct MP particle showing visible polymer coating or inclusion within a chitosan-rich cluster during SEM counting.

3. Results and discussion

3.1. Chemical characterization (^{1}H-NMR)

The chemical identity and DDA of the four chitosan variants were established *via* ^{1}H-NMR spectroscopy (Fig. 1). All spectra displayed the characteristic signals of the chitosan backbone: the multiplex signals between δ 3.4 and 4.0 ppm correspond to the protons H2–H6 of the glucopyranose ring, while the signal at $\delta \approx 3.1$ ppm is assigned to the H2 proton of the glucosamine unit. The resonance at $\delta \approx 4.8$ ppm (partially overlapped by the D_2O signal) corresponds to the anomeric proton H1. The DDA was calculated by comparing the integral of the residual acetyl group methyl protons (CH_3 at $\delta \approx 2.0$ ppm) with the integral of the H2–H6 signals. The calculated DDA values were 84.2%, 82.5%, 90.8%, and 87.6% for Chito 1, 2, 3, and 4, respectively. The observed entrapment differences are essentially controlled by the hydrodynamic volume and macromolecular diameters of the chains, rather than being an artifact of various electrostatic attractions, due to the consistency in DDA among samples ($>80\%$).

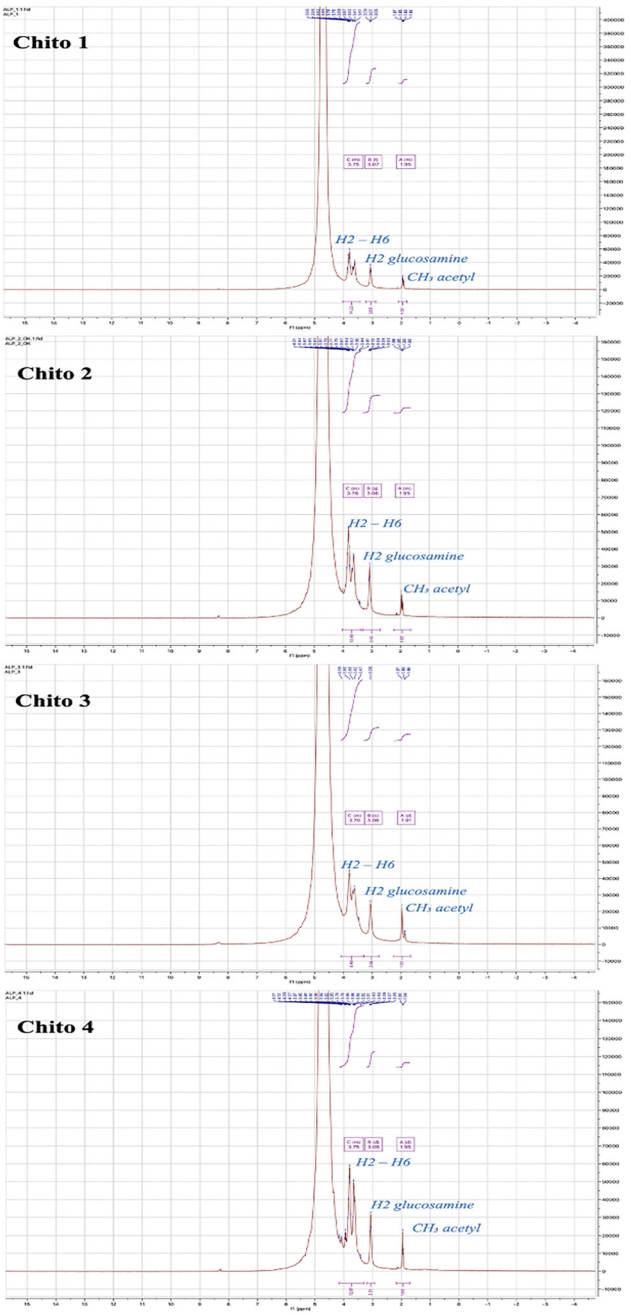

Fig. 1 ^{1}H-NMR spectra (400 MHz, D_2O/CD_3COOD) of the four chitosan variants used in this study.

Notably, the spectra for Chitosan 3 (extracted from *Procambarus clarkii*) showed a remarkably clean baseline and well-defined peaks, confirming the high efficiency of the deproteinization and demineralization steps. The fact that all variants possess a consistently high DDA ($>80\%$) allows us to conclude that the differences in MP entrapment efficiency are primarily governed by the macromolecular architecture of the chain length and hydrodynamic volume rather than variations in surface charge density.

The ^{1}H-NMR spectrum of Chito 1 exhibits a typical, slightly complex profile, according to Fig. 1. Chito 2's spectrum has a lower DDA and more signal dispersion. Chito 3 has the cleanest spectrum with well-defined peaks and the highest DDA. Lastly, Chito 4's spectrum features a somewhat well-defined intermediate profile (Fig. 1).

3.2. Thermal characterization (TGA)

Thermogravimetric analysis (TGA) was used to further assess the chitosan variants' structural integrity. All samples exhibited a two-step weight loss profile: an initial dehydration phase (50–120 °C) followed by a major thermal degradation event starting at $\approx$260 °C, corresponding to the depolymerization of the polysaccharide backbone. The thermal stability of Chito 3 and Chito 4 was significantly higher ($T_{max} \approx 310$ °C) than that of the low-viscosity variants (Fig. 2). The formation of the dense polymeric networks required to prevent MP entrapment is facilitated by this increased thermal resistance, which is correlated with their elevated molecular weight and suggests a more organized crystalline structure.

According to the typical curves in Fig. 2 (N_2 atmosphere) and Fig. 3 (Air atmosphere) and the standard behaviour of chitosan samples, Zone 1 (50–120 °C) exhibits the loss of bound water (moisture). Due to a denser hydrogen bond network, the higher viscosity chitosans (Chito 3 and Chito 4) typically hold onto slightly more water. The primary thermal degradation (chain breakage and deacetylation) occurs in Zone 2 (250–350 °C). Adsorbed water evaporates at Zone 1 (50–120 °C), resulting in a mass loss of roughly 8–12%. The thermal degradation of the pyranose rings and the deacetylation process are represented by zone 2 and the most significant stage (260–380 °C). Indirect evidence of a higher molecular weight and a more ordered network structure can be found in Chito 3 and Chito 4's slightly higher peak of maximum rate (T_{max}) or onset of degradation (T_{onset}) compared to the lower viscosity chitosans. This shift suggests that greater DDA and molecular weight are inherently associated with the higher intrinsic viscosity seen in Chito 3 and Chito 4. Additionally, the air environment analysis revealed

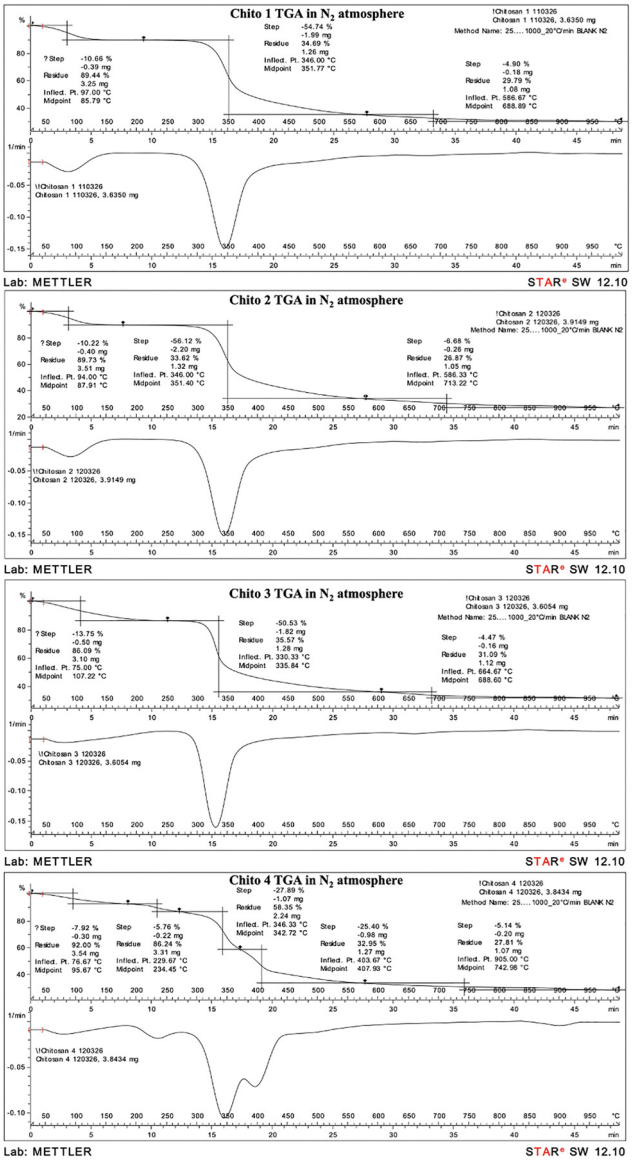

Fig. 2 TGA thermograms (N_2 atmosphere) of the four chitosan variants used in this study. The T_{max} for the main degradation stage is highlighted by the dashed lines, indicating the derivative weight loss (DTG) curves. The formation of stable semi-dilute entangled networks is supported by Chito 3 and Chito 4's increased thermal stability. Comparative TGA curves in a N_2 atmosphere for Chito 1, Chito 2, Chito 3, and Chito 4, showing the increased thermal stability of the high-viscosity variants.

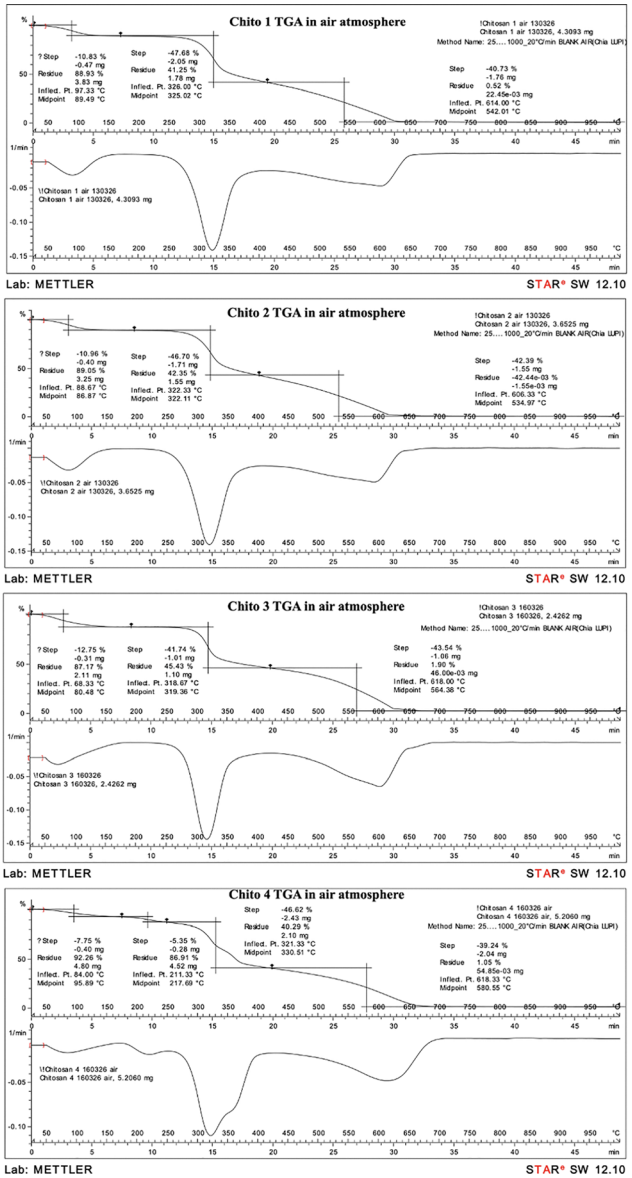

Fig. 3 TGA thermograms (air atmosphere) of the four chitosan variants used in this study. The dashed lines represent the derivative weight loss (DTG) curves, highlighting the T_{max} for the main degradation stage. The higher thermal stability of Chito 3 and Chito 4 supports their ability to form stable semi-dilute entangled networks. TGA and DTG profiles of Chito 3 in air atmosphere, confirming high purity and complete combustion of the organic matrix.

no residue in any of the samples, demonstrating the exceptional purity of Chito 3 and the lack of notable inorganic pollutants. In terms of the atmosphere (N_2 *vs.* air), complete combustion may take place during air, whereas just a carbonaceous residue (char) is left in nitrogen (Fig. 2 and 3).

To determine an association between the macromolecular structure and entrapment efficiency of the four chitosan variations, their thermal stability was assessed. Every sample displayed a two-step weight loss curve, illustrated in Fig. 2 and 3. The first stage (50–120 °C) is associated with an 8–11% loss of adsorbed water. Thermal breakdown of the saccharide rings and deacetylation occur during the second and essential stage (270–390 °C). In comparison to Chito 1 (298 °C), Chito 3 and Chito 4 demonstrated exceptional thermal resistance, with maximum degradation temperatures (T_{max}) of 314 °C and 316 °C, respectively. Stronger inter-chain hydrogen bonds and a higher DDA are indicated by this positive shift in T_{max}. All samples undergo near-total combustion with minimal residual ash (<1.5%) under oxidative circumstances (air), demonstrating the high purity of the Chito 3 derived from *Procambarus clarkii* (Fig. 3). These results confirm the theory that the enhanced structural integrity of these high-molecular-weight

polymers, which may preserve a stable semi-dilute entangled network during simulated gastric shear, is the reason for the ''threshold effect'' observed at ≥90 cP.

Regarding the curve behaviour in Fig. 2 and 3, it can be observed that there is a slight initial decline (water loss) in Zone 1 (50–120 °C). During this phase, the four chitosans' curves are typically considerably close to each other. Each chitosan's ''fingerprint'' is observable in Zone 2 (270–380 °C). As a result, Chito 1's curve, which is the weakest, declines first (the curve farthest to the left). Chito 3 and Chito 4's curves have been adjusted to the right, and thus are more stable.

Indirect evidence of the formation of a denser, more ordered hydrogen-bonded network can be observed in the positive shift in T_{max} for Chito 3 and Chito 4 (>310 °C). High-viscosity variations are able to maintain a stable physical mesh around MPs even in acidic stomach circumstances because of their structural stability.

In conclusion, intrinsic viscosity and heat stability are directly correlated across all four chitosan grades, according to the physicochemical characterization presented in Table 2. Although Chito 4 has the highest value viscosity and T_{max}, Chito 3's higher DDA (90.8%) provides the best compromise for MP entrapment. Consequently, Chito 3 has been found to be the most suitable for MP remediation applications due to its enhanced surface reactivity and durable structural characteristics.

3.3. SEM morphological evidence of the threshold effect of chitosan viscosity on MP binding

Considering that ^{1}H-NMR demonstrates that all chitosan samples have similar levels of deacetylation (82–91%), it is reasonable to rule out variations in electrostatic charge density as the primary mechanism controlling MP interaction. Actually, the high correlation between entrapment efficiency, contour length, molecular weight, and inherent viscosity suggests that chain overlap and macromolecular architecture are the main factors influencing the observable behaviour.

All chitosan samples were completely soluble under the experimental settings (pH = 3), even though MW affects chitosan solubility (Table 1). Thus, the limiting factor controlling the blending of chitosan and MPs was not solubility. Rather, the ability of chitosan to form extensive networks and establish multipoint interactions with particle surfaces was determined by its intrinsic viscosity and polymer chain length, which relate to blending efficiency. While high-molecular-weight chitosan builds continuous polymeric meshes that can physically trap MPs, low-molecular-weight chitosan stays molecularly scattered and acts as isolated chains. Thus, combining behavior is regulated by the creation of networks rather than solubility *per se*.

Table 2 Physicochemical characterization of chitosan samples

Sample	Intrinsic viscosity (cP)	DDA (%) by ^{1}H-NMR	T_{max} TGA (°C)
Chito 1	≈20	84.2	298
Chito 2	≈64	85.2	302
Chito 3	≈112	90.8	314
Chito 4	≈250	87.6	316

The interaction between chitosan and MPs as a function of inherent viscosity exhibited distinct and reproducible morphological changes, according to SEM analysis. Crucially, the observed differences were not progressive but rather suggested a threshold-like shift in the polymer phase's structural structure.

Semi-quantitative image analysis, including aggregate size distribution and cluster density over several fields, was added to the SEM findings to bolster this finding. The observed morphological transition is consistent with a quantifiable structural reorganization rather than merely qualitative variations, as these parameters demonstrated a rapid increase above the 90 cP threshold.

Chitosan samples with low viscosity (10–80 cP) exhibited mostly scattered polymer chains with little contact with MP surfaces. With only sporadic and irregular polymer adsorption under these circumstances, MPs remained mostly exposed, which is consistent with a diluted regime where polymer chains act unimpeded. High-viscosity chitosan samples (≥90 cP), on the other hand, exhibited the formation of extended, continuous polymeric networks that enveloped both individual MPs and MP clusters.

These networks produced compact composite aggregates by connecting many particles and filling interstitial areas with filamentous and amorphous characteristics. The existence of a critical threshold linked to polymer chain overlap and entanglement is supported by the quick rather than gradual transition between these two regimes.

It is crucial to clarify that intrinsic viscosity should be understood as an experimentally accessible stand-in for the hydrodynamic volume and chain overlap of the polymer rather than as an independent causative variable. Therefore, the transition from isolated chains to an entangled semi-dilute regime, whereby inter-chain connections allow the generation of continuous networks capable of topologically restricting MPs, is more fundamentally connected to the observed threshold behaviour.

Low-viscosity chitosan (10–80 cP) showed negligible binding (0–7%). High-viscosity chitosan (≥90 cP) displayed strong binding across all MP types. In this instance, intrinsic viscosity must be defined as a stand-in for the chain overlap concentration (c^*). The system operates in a dilute regime below 90 cP, when chains function as isolated coils with insufficient reach to connect several MP surfaces. The semi-dilute entangled phase, where inter-chain entanglements provide the mechanical structure required to withstand the shear pressures of simulated stomach churning, begins at ≥90 cP. Macromolecular entanglement and interpolymeric bridging control the modification from marginal binding to widespread trapping at the 90 cP threshold. The observed threshold at ≥90 cP suggests a transition from a dilute regime, where isolated chitosan chains merely adsorb to the MP surface, to a semi-dilute entangled regime. In this state, the polymer contour length (≥310 nm) is sufficient to bridge multiple particles, creating a robust physical mesh capable of resisting gastric shear forces.

Viscosity is a direct indicator of chitosan's hydrodynamic volume and contour length. The contour lengths of Chitosan 1 and Chitosan 2 (< 80 cP) were excessively short (< 300 nm) to completely fill the holes between different plastic particles.[19]

A MW of no less than 100 kDa and a degree of polymerization of around 600 monomers are linked with a viscosity of at least 90 cP, allowing for the creation of a continuous polymeric mesh compared to isolated strands. Multipoint interactions can be established by chitosan at this essential contour length. Short chains don't have enough length to entangle with nearby polymer chains, but they might make a few hydrogen bonds with MPs. The mechanical stability required for enduring stomach shear forces (30 rpm) was provided by high-viscosity networks (90–400 cP). The minimal entrapment observed for Chitosan 1 and 2 was explained by the initial binding remaining too weak to withstand dissociation below this threshold.

SEM imaging showed that high-viscosity chitosan formed visible filamentous or amorphous coatings surrounding MPs of HDPE, PVC and PET (Fig. 4 to 6).

Using surface texture analysis, the morphological differences between the polymer matrix and the MPs were identified. High-viscosity chitosan (Chito 3 and 4) appeared as a continuous fibrillar network or an amorphous covering encasing these particles, whereas the cryo-ground MPs (HDPE, PVC, and PET) exhibited multiple and sharp-edged fractured surfaces. Due to the dispersed nature of oxidation sites on the plastic surfaces created during the grinding process, the observed interaction ranged from total encapsulation to surface adhesion. SEM images under all settings were displayed at standard magnifications to provide a meaningful comparison.

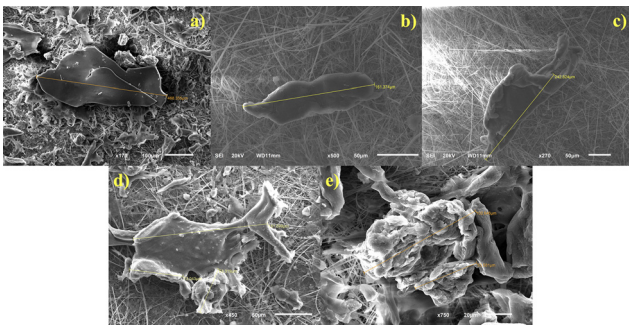

Fig. 4 SEM images of the bond between chitosan and HDPE-MPs: (a) HDPE-MP without chitosan, (b) HDPE-MP after the addition of Chito 1 at 1.0 mg mL^{-1}, (c) HDPE-MP after the addition of Chito 2 at 1.0 mg mL^{-1}, (d) HDPE-MP after the addition of Chito 3 at 1.0 mg mL^{-1}, and (e) HDPE-MP after the addition of Chito 4 at 1.0 mg mL^{-1}.

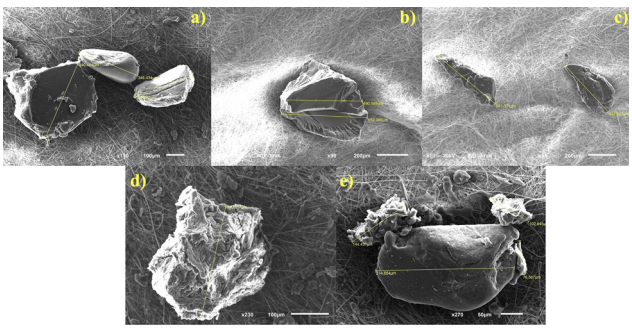

Fig. 5 SEM images of the bond between chitosan and PVC-MPs: (a) PVC-MP without chitosan, (b) PVC-MP after the addition of Chito 1 at 1.0 mg mL^{-1}, (c) PVC-MP after the addition of Chito 2 at 1.0 mg mL^{-1}, (d) PVC-MP after the addition of Chito 3 at 1.0 mg mL^{-1}, and (e) PVC-MP after the addition of Chito 4 at 1.0 mg mL^{-1}.

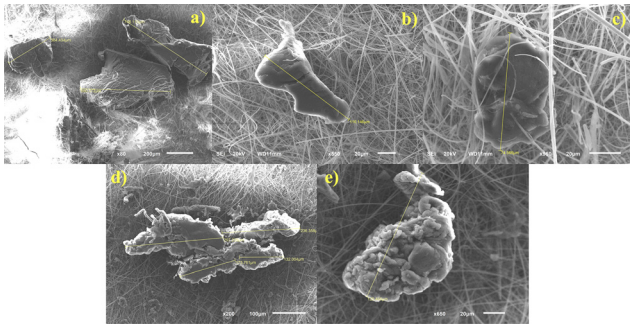

Fig. 6 SEM images of the bond between chitosan and PET-MPs: (a) PET-MP without chitosan, (b) PET-MP after the addition of Chito 1 at 1.0 mg mL^{-1}, (c) PET-MP after the addition of Chito 2 at 1.0 mg mL^{-1}, (d) PET-MP after the addition of Chito 3 at 1.0 mg mL^{-1}, and (e) PET-MP after the addition of Chito 4 at 1.0 mg mL^{-1}.

When HDPE, PVC, and PET MPs accumulate, SEM analyses of polymer aggregation indicate the creation of polymer-rich networks around particle clusters rather than weak interaction. Aggregation in high-viscosity chitosan samples was associated with the formation of continuous polymeric matrices that encapsulate MPs, which were consistent with physical entrapment as opposed to simple surface adsorption. Low-viscosity chitosan, on the other hand, exhibited polymer aggregation without stable particle inclusion, suggesting that a short chain length inhibits the development of long-lasting interpolymeric bridges between MPs. High-viscosity chitosan (≥ 90 cP) encapsulated individual MPs and MP clusters in continuous filamentous and amorphous polymeric layers, as evidenced by SEM imaging. These coatings created compact composite structures by filling interstitial spaces and linking nearby particles with interconnected fibrillar networks. Low-viscosity chitosan samples lacked these characteristics, with MPs being mostly exposed and spatially isolated from the polymer phase. Interestingly, these coatings were absent when using low-viscosity chitosan or MPs alone. In brief, SEM analysis revealed polymer networks surrounding MPs only in Chito 3 and Chito 4 samples, while Chito 1 and Chito 2, despite identical deacetylation, lacked the polymeric length and hydrogen-bonding density necessary to form stable interpolymeric networks. This indicates a threshold effect rather than a gradual efficacy gradient.

The hydrogen-bonding density differed due to variability in the length of the polymer chain and the spatial distribution of functional groups along the chain structure, even though the polymer concentration and DDA remained constant across samples. Longer polymer chains increase the probability of

multipoint hydrogen bonding with particle surfaces and nearby polymer chains due to them containing more accessible hydroxyl and amino groups within a single macromolecule. Consequently, regardless of the same chemical composition, high-viscosity chitosan produces larger effective hydrogen-bond concentrations per interaction area.

Polymer chain length and intrinsic viscosity cooperate to yield the estimated sequestration efficiency. The hydrodynamic volume and MW of the polymer directly affect intrinsic viscosity, according to the Mark–Houwink interaction.[18] The polymer chains (length $\geq$310 nm) shift from a diluted regime to a semi-dilute entangled network at the specified threshold ($\geq$90 cP). The structural framework required to physically restrict MPs is provided by this macromolecular entanglement, while shorter chains (Chito 1 and Chito 2) remain distinct strands with inadequate contour length to bridge several particles.

It is crucial to emphasize that the aim of this study's SEM analysis is to enable a reliable comparative evaluation of polymer–particle organization under various conditions rather than to offer precise quantitative surface coverage. The statistical significance of the observed differences is ensured by a combination of semi-quantitative analysis of images (aggregate size and cluster density), consistency across triplicates, consistent scoring criteria, and systematic field sampling ($\geq$45 fields per condition). Crucially, the validity of the morphological interpretation is reinforced by the excellent correlation ($R^2 >$ 0.85) between these image-derived parameters and independent mass-based recovery measurements.

3.3.1. SEM analysis confirmation. Stereomicroscopy corroborated the SEM findings (Table 3). Chito 3, and Chito 4 promoted clustering and partial encapsulation or, dense coatings, while Chito 1 and Chito 2 were almost ineffective. Concentrations of MPs from 0.5 mg L^{-1} to 1 mg L^{-1} were efficiently bound by Chito 3 and Chito 4 (between 65% to 87% of binding) while almost no binding was present for Chito 1 and Chito 2. Increasing the concentration to 2 mg L^{-1}, the binding with Chito 3 and Chito 4 is only slightly reduced (at least 42% of binding) and no binding was shown with Chito 1 and Chito 2.

The qualitative scoring (0–2) was validated by the quantitative recovery of MPs *via* filtration, showing a direct correlation ($R^2 >$ 0.85) between visual cluster density and mass-based binding. The SEM image scoring was identical for HDPE, PVC, and PET despite structural differences because chitosan viscosity rather than MP chemical composition was the main indicator of binding. Regardless of the polymeric makeup of the MPs, high-viscosity chitosan created vast polymeric networks that were able to trap them. This indicates that polymer chain length and network-forming ability, rather than the specific surface chemistry of the MPs, were the main factors controlling the contact process.

Table 3 SEM image scoring (% binding)[a]

Polymer	Chito 1	Chito 2	Chito 3	Chito 4
HDPE	0	0	2	2
PVC	0	0	2	2
PET	0	0	2	2

[a] 0 = no binding; 1 = moderate binding (10–20 events/quadrant): and 2 = extensive binding (>20 events).

The transition observed in Table 3 corresponds to a significant shift in the spatial distribution of polymer networks rather than a gradual variation, as confirmed by the semi-quantitative conversion of SEM scoring into cluster density (events per field), which indicated a sharp increase above the 90 cP threshold (Fig. S1).

In addition, from the binary-like transition observed in Table 3, image analysis confirmed that high-viscosity chitosan samples exhibited significantly larger aggregate diameters and higher cluster densities in comparison to low-viscosity variants. The semi-quantitative SEM scoring (Table 3) consistently distinguished between low- and high-viscosity chitosan samples across all MP types (HDPE, PVC, PET). Chito 3 and Chito 4 showed extensive network formation and particle embedding (score = 2), while Chito 1 and Chito 2 exhibited negligible interaction (score = 0). This binary-like response further supports the presence of a threshold mechanism rather than a continuous gradient of interaction strength. Importantly, the consistency of scoring across multiple fields and independent replicates reinforces the robustness of the observed trend.

Importantly, the aim of this study is not to quantify absolute surface coverage, but to identify a regime transition in polymer–particle interaction, for which comparative morphological analysis is both sufficient and appropriate.

3.4. Mechanistic justification and physiological significance

3.4.1. Binding mechanism. It should be observed that this regime transition is inferred indirectly from viscosity–structure–function correlations rather than directly measured *via* rheological parameters like overlap concentration (c^*) or viscoelastic moduli (G', G''). Nevertheless, the understanding of the threshold effect in terms of a transition from a dilute to semi-dilute entangled regime is consistent with classical polymer physics.

The acidic stomach environment during a meal was taken into consideration for chitosan binding to MPs.[10] When food is consumed, MPs interact with chitosan in the stomach and progressively go to the duodenum as a component of the gastric chyme. According to Guan *et al.*,[20] the analyzed quantities match standard supplemental chitosan dosages of 0.5–1 g day^{-1}, which generate luminal concentrations of 0.5–1 mg mL^{-1} in the stomach.[21] Across typical dietary exposure levels, these quantities are suitable for considerable MP binding.

Instead of engaging chemically in the sense of specific molecular recognition, chitosan and MPs interact in a structurally selective manner. The physicochemical characteristics of the polymer network (polymer length, hydrodynamic volume, and multipoint interaction capacity) and the plastic surface's accessibility regulate binding. Regardless of the chemical load MPs may be carrying, high-viscosity chitosan creates long interpolymeric networks that physically trap MPs. The three-dimensional polymeric mesh created by chitosan–chitosan interactions is referred to as an ''interpolymeric network''.[10]

MPs may then be integrated into this network through surface contacts and physical entrapment (topological entrapment). MPs function as inert inclusions embedded inside the chitosan matrix, whereas polymer–polymer interactions drive network creation. Co-transported chemicals do not prevent entrapment since the interaction occurs with the plastic surface itself, not with adsorbed organic or inorganic pollutants. Consequently, instead of affinity for particular molecular species, selectivity results from geometric and topological compatibility between polymer chains and particle surfaces.[10]

PVC may exhibit polarized C–Cl bonds and oxidized surface defects generated during processing and grinding, whereas PET contains ester carbonyl and ether oxygen atoms that may act as hydrogen-bond acceptors. Despite being essentially non-polar, HDPE may exhibit oxidized functionalities (such as hydroxyl and carbonyl groups) that are created during cryo-grinding and environmental deterioration.

Chitosan's amino groups are protonated in stomach pH settings, although hydrogen bonding may continue through hydroxyl groups and electrostatic stabilization of polymer–surface contact, which promotes topological entrapment and a semi-dilute entangled polymer regime.[22] All samples have a similar cationic potential (high DDA), but only those that reach the 90 cP threshold (Chito 3 and Chito 4) have the essential chain entanglement density to accomplish effective MP entrapment, according to the combination of NMR and viscometric data. The initial electrostatic approach to the MPs is facilitated by the high DDA, which guarantees that the main amine groups (NH_3^+) are fully protonated at pH 3.0. Nevertheless, the ^{1}H-NMR data suggest that charge is not sufficient for sustained sequestration; the long-range inter-chain interactions supplied by the high-molecular-weight fractions observed in Chito 3 and Chito 4 are crucial for the mechanical "caging" of MPs.

According to Dambusa *et al.*,[23] the flexible polymer chain permits multipoint contacts, which lead to topological entrapment. Stable entanglement or networks with MP surfaces require a polymer length of around 310 nm and intrinsic viscosity of not less than 90 cP (about 600 monomers). The main benefits of this binding mechanism are as follows: (a) non-selective, effective against several kinds of plastics (HDPE, PVC, PET); (b) safe because chitosan is well tolerated; (c) robust, with binding persisting over physiological pH ranges; (d) scalable due chitosan manufacturing being well-established; and (e) innovative, targeting MPs in a dietary context.

At a degree of deacetylation of roughly 85%, chitosan possesses a strong polycationic property due to its high density of protonated amino groups in acidic conditions.[24] Therefore, a mixture of non-covalent forces, such as hydrogen bonding, van der Waals interactions, and physical entanglement of polymer chains surrounding particle surfaces, promote blending with MPs. Additionally, chitosan's flexible backbone promotes a semi-dilute entangled polymer regime and mechanical interlocking by allowing conformational adaptability to surface irregularities of MPs. When MP surfaces have polar or oxidized functional groups, electrostatic interactions might play a crucial role. Despite the lack of covalent bonding, these combined forces produce stable polymer–particle complexes.

While specific molecular recognition is absent, the binding is driven by topological entrapment. The high cationic charge density of chitosan at pH 3.0 facilitates initial electrostatic approach to oxidized MP surfaces, but the long-term stability of the complex is maintained by the mechanical interlocking of the high-molecular-weight chains.

Additionally, the suggested binding mechanism increases the likelihood of even stronger interactions among chitosan and environmentally weathered MPs. The density of surface-active functional groups, such as carbonyl and carboxyl moieties, on plastic particles is increased by aging caused by atmosphere and/or UV light. The higher hydrophilicity of aged MPs would probably improve the density of the semi-dilute entangled polymer regime and the overall stability of the resulting complexes, since the topological entrapment process heavily depends on hydrogen bonding and electrostatic stabilization between the chitosan's amino/hydroxyl groups and the MP surface.[25]

From a methodological standpoint, the hypothesized technique is coherently validated on multiple scales by combining independent mass-based measurements with semi-quantitative SEM analysis, which connects macroscopic entrapment efficiency with morphological observation.

3.4.2. Physiological relevance. Chito 3 and Chito 4 efficiently bind MPs in acidic conditions, mimicking the stomach environment.[6,8] When partially buffered meals are included, the pH of the stomach usually stabilizes at 3.0 during digestion. This pH is a physiologically suitable intermediate level that reduces variability and conforms with previous findings. According to Rondanelli *et al.*,[26] chitosan may establish networks with dietary lipids and carbohydrates. The polymer's MW is essential because smaller polymers establish weakened networks, whereas larger polymers entangle to create stable networks that may include MPs. Other phases of digestion, like duodenal transit (pH 5–6), were not considered because the study concentrated on gastric retention and biofilm formation. The purpose of the experiment was to isolate the impact of chitosan viscosity on particle entrapment by simulating the stomach's acidic environment (pH = 3.0). The model accurately represents the stomach phase of digestion, where the initial polymer–MP complexes form, even if it excludes bile salts and digestive enzymes to minimize biological interference. To simplify the model, gastric enzymes like lipases were deliberately left out. Gastric amylases are inactive at this pH, while gastric lipases are minimally active and have very limited ability to degrade chitosan. Combining NMR, TGA, and viscometric data provides a thorough structural understanding for the "threshold effect" that has been identified. The TGA and viscosity studies show significant variations in the physical robustness of the four chitosans, even if NMR indicates that they all have a similar chemical identity and high cationic potential (DDA $\approx$ 82–91%). For Chito 3 and Chito 4, the shift in T_{max} toward higher temperatures is consistent with their greater intrinsic viscosity ($\geq$90 cP), indicating that these variants have the crucial chain

length ($\geq$ 310 nm) essential for the transition from simple surface adsorption to a stable semi-dilute entangled network. Consequently, the entrapment of HDPE, PVC, and PET is a purely topological event rendered accessible by the macromolecular structure of the high-molecular-weight chitosan rather than a unique chemical functionalization.

3.4.3. Formulation considerations. For MP capture, an efficient matrix should include lipid-based hydrophobic adhesion, starch-based porosity/viscoelastic control, and cationic chitosan-facilitated electrostatic attraction. Compared to chitosan alone, composite chitosan–starch–lipid networks are more effective at trapping MPs.[27,28] Particularly in turbulent flow, finer meshes enhance the chance of getting into contact with heterogeneous MPs, especially particles smaller than 100 μm. Modified viscosity/porosity (starches) and improved adhesion (lipids) are two advantages of co-formulation. Polyelectrolyte complex formation and ionic gelation are rendered simpler by chitosan with low to moderate viscosity.

Hydrogen bonding and electrostatic interactions with negatively charged surfaces are facilitated by high cationic charge, which is generated by protonation in acidic conditions. DDA at higher levels intensifies this effect. While networks with a viscosity of 250–450 cP perform well in static applications, capturing larger particles and enduring shear forces, networks with a viscosity of 90–120 cP are typically more effective in dynamic circumstances. The most effective chitosan networks for MP retention are chosen based on the criteria provided in Table S1.

3.4.4. Implications for MP exposure. MP entrapment decreases systemic translocation, luminal mobility, uptake, and epithelial contact. These results suggest the development of chitosan-based dietary supplements or pharmaceutical formulations that reduce human exposure to MPs. Based on the cryo-grinding and sieving parameters, the study's objective is strictly restricted to MPs in the 100–500 μm size range.[4,29,30]

3.5. Physiological complexities and food matrix interference

Although the current study shows the fundamental physicochemical parameters governing chitosan–MP binding, gastrointestinal mechanics and the food matrix must be taken into account when converting these *in vitro* results to a clinical or nutritional setting. Gastric motility and peristaltic shear pressures may have an impact on the mechanical stability of the chitosan–MP aggregates under physiological conditions. The complex turbulent flow of the human stomach may affect the rate of network creation and aggregation stability, even though the experimental agitation (30 rpm) simulates mild gastric mixing.[8,14,20] Additionally, the co-ingestion of MPs with a complex dietary matrix including proteins, lipids, and other polysaccharides offers a more plausible situation. Dietary lipids and carbohydrates are known to interact with chitosan, perhaps resulting in competitive binding.[13,16] This "food effect" may improve topological entrapment by creating composite chitosan–lipid–starch networks that raise the total luminal viscosity and hydrophobic adhesion, or it may decrease MP capture by competitively occupying chitosan's active sites.[4,9,11] To determine how these mechanical and biochemical factors influence the effectiveness of chitosan as a dietary interceptor for plastic pollutants, future *in vivo* studies along with investigation using standardized food models are essential.[12]

4. Study limitations

Despite recognizing that this study clearly establishes a physicochemical threshold for chitosan-MP interaction, a number of limitations need to be mentioned: (a) physiological complexity: the potential of competitive binding or enzymatic breakdown by pepsin or stomach lipases is eliminated by using a simplified electrolyte-free gastric model (pH 3.0). Even though these enzymes minimally break down chitosan at this pH, their presence may slightly change the surface tension of the network; (b) gastric motility: the complicated peristaltic shear pressures and turbulent flow of the human stomach may impact the mechanical durability of the larger chitosan-MP aggregates, even if our experimental agitation (30 rpm) models moderate mixing; (c) food matrix interference: consuming a complex meal that contains proteins, lipids, and starches at the same time may cause concurrent occupancy of chitosan's active sites, which could alter the sequestration efficiency described here; (d) size range: the 100–500 μm fraction was the sole topic of this study; (e) resolution of the viscosity threshold: accurately identifying the key transition region is limited by the use of four discrete viscosity values. To more precisely characterize the percolation threshold and explicitly verify the commencement of the semi-dilute entangled regime, a more accurate viscosity gradient (especially in the 80–120 cP range) in conjunction with rheological characterization would be essential.

It is yet unclear how small MPs or nanoplastics (NPs) act, which could include various interfacial kinetics (*i.e.*, Brownian motion *vs.* gravitational settling).

According to recent studies, MPs—including aggregated or surface-modified particles—may still be absorbed by the intestines under specific circumstances.[12,31] As a result, absorption is not always prevented by the creation of MP–chitosan complexes, and more research is essential to establish their biological fate. Recent study evidence suggests that even aggregated MPs may be absorbed at the intestinal level, indicating that the presence of chitosan doesn't guarantee that particle uptake is completely avoided. The need to distinguish between physicochemical entrapment mechanisms and biological uptake processes—which are controlled by variables other than polymer–particle interactions—is further supported by the recently published findings.[12,31]

Conclusions

The efficient sequestration of HDPE, PVC, and PET MPs by chitosan under simulated stomach settings has been determined to have a crucial physicochemical threshold. Our findings indicate that the rheological ability to create robust physical networks is limited to chitosan variations with an

intrinsic viscosity of ≥90 cP, which corresponds to a molecular weight of ≥100 kDa and a polymer contour length of ≥310 nm.

Topological entrapment in a crosslinked polymer regime drives MP sequestration, according to mechanical data backed by SEM and TGA, with Chito 3 representing the most effective variant. Chito 3 is preferable due to its structural balance, even though ^{1}H-NMR analysis showed a consistently high DDA (82–87%) across all samples, guaranteeing adequate cationic charge density. The higher thermal stability of Chito 3 (T_{max} = 315 °C), which exhibits similar surface chemistry, confirms that its chain length is optimal for bridging particles under shear more effectively than lower molecular weight variants. Intrinsic viscosity, the first quantitative physicochemical parameter for the design of dietary interceptors of MPs, was determined in this study. Additionally, Chito 3 promotes better gastric entrapment (pH 3.0) before the duodenum's sol–gel transition (pH 6.0–7.0). At this stage, an irreversible "block" of MPs in a solid precipitate develops by the deprotonation of amino groups, as determined by NMR. The most promising functional dietary interceptor for reducing MP bioavailability and increasing fecal excretion is thereby determined to be Chito 3.[12] These findings additionally establish the foundation for future *in vivo* assessment and enhancement of chitosan-based treatments for treating dietary plastic pollutants.

Author contributions

C. C.: conceptualization, methodology, visualization, formal analysis, writing original – draft, and writing – review and editing; S. B.: visualization, methodology, and writing original – draft; R. L.: visualization, methodology, and writing – review and editing; U. C.: visualization, methodology, writing original – draft, and writing – review and editing.

Conflicts of interest

The authors declare that they have no known competing financial interests or personal relationships that could have appeared to influence the work reported in this paper.

Data availability

The data that support the findings of this study are available from the corresponding author, C. C., upon reasonable request.

Supplementary information (SI) is available. See DOI: https://doi.org/10.1039/d6tb00654j.

Acknowledgements

The authors are thankful to the Photonic Microscopy and Image Processing Unit of the Scientific and Technical Services of the University of Oviedo (Confocal UniOvi ImageJ) for guidance with the SEM and stereomicroscopy analysis of MPs. The authors are thankful to the Faculty of Chemistry of the University of Pavia for guidance with the ^{1}H-NMR and TGA analysis of chitosans.

References

1 C. Vitali and F. S. Ruggeri, *Adv. Chem. Pollut. Environ. Manage. Protect.*, 2025, **13**, 179–217.
2 S. Jayavel, H. Govindaraju, J. R. Michael and B. Viswanathan, *Bull. Nat. Res. Cent.*, 2024, **48**, 110.
3 L. Zhou, L. Ran, Y. He and Y. Huang, *Mol. Med. Rep.*, 2025, **31**, 98.
4 C. Casella, D. Dondi and D. Vadivel, *Environ. Pollut.*, 2025, 127343.
5 K. N. Lazaridis, C. Koutsari and R. M. Samsonraj, *Gastro. Hep. Adv.*, 2025, **4**(8), 100694.
6 U. Cornelli and P. Morganti, *J. Appl. Cosmetol.*, 2014, **32**(1/2), 21/28.
7 W. Wang, C. Xue and X. Mao, *Int. J. Biol. Macromol.*, 2020, **164**, 4532–4546.
8 J. Zhang, R. Zhang, P. Wang, P. Wen, W. Zhang, S. Liu and F. Ren, *Food. Chem. X.*, 2025, **31**, 103014.
9 H. Kwon, J. Choi, C. Lim, J. Kim, A. Osman, Y. Jho, D. S. Hwang and D. W. Lee, *Biomacromolecules*, 2025, **26**, 1012–1022.
10 C. Casella, U. Cornelli, S. Ballaz, G. Zanoni and L. Ramos-Guerrero, *Polymers*, 2025, **17**, 1445.
11 H. Ullah, H. Chang, N. A. Safi, B. Somia, J. Wang, A. Qiao and R. Su, *Carbohyd. Polym.*, 2025, 124073.
12 C. Casella, U. Cornelli, S. Ballaz, M. Recchia, G. Zanoni and L. Ramos-Guerrero, *Foods*, 2025, **14**, 2190.
13 S. Affes, I. Aranaz, N. Acosta, Á. Heras, M. Nasri and H. Maalej, *Biomass Conv. Bioref.*, 2024, **14**(3), 4111–4121.
14 K. Ahmad, Y. Zhang, P. Chen, X. Yang and H. Hou, *Carbohydr. Polym.*, 2024, **333**, 121926.
15 U. Cornelli, C. Casella, G. Belcaro, M. R. Cesarone, S. Marucci, M. Rondanelli, M. Recchia and G. Zanoni, *Microplastics*, 2025, **4**, 93.
16 G. M. Pavlov and A. A. Gosteva, *Polym. Sci.*, 2022, **64**, 586–590.
17 U. Cornelli, G. Belcaro, M. Recchia and N. D'Orazio, *Curr. Develop. Nutr.*, 2017, **1**, e000919.
18 M. R. Kasaai, *Carbohyd. Polym.*, 2007, **68**(3), 477–488.
19 J. Qian, X. Wang, Y. Chen, C. Mo, C. Liang and H. Guo, *Carbohydr. Res.*, 2023, **530**, 108860.
20 G. Guan, M. A. K. Azad, Y. Lin, S. W. Kim, Y. Tian, G. Liu and H. Wang, *Front. Physiol.*, 2019, **10**, 516.
21 M. Kubbinga, M. A. Nguyen, P. Staubach, S. Teerenstra and P. Langguth, *Pharm. Res.*, 2015, **32**, 2241–2249.
22 A. Anwar, M. Imran, M. F. Warsi, I. A. Alsafari, R. Parra-Saldívar, G. Gutiérrez-Soto and H. M. Iqbal, *Front. Mater.*, 2025, **12**, 1588627.
23 A. Dambuza, P. P. Mokolokolo, M. E. Makhatha and M. A. Sibeko, *Polymers*, 2025, **17**, 2447.
24 C. Carrera, C. Bengoechea, F. Carrillo and N. Calero, *Food Hydrocoll.*, 2023, **137**, 108383.

25 K. Bhagat, A. C. Barrios, K. Rajwade, A. Kumar, J. Ostwald, O. Apul and F. Perreault, *Chemosphere*, 2022, **298**, 134238.
26 M. Rondanelli, S. Perna, M. D. Porta, F. Lombardoni, Z. Patelli, M. Nichetti and R. Cazzola, *BMC Nutr.*, 2025, **11**(1), 170.
27 C. Kiki, E. D. Ahlonsou, K. Chabi and A. B. E. Adéoyé, Persistent Organic Pollutants from Plastics: Sources, Environmental Monitoring, *Toxicity, and Remediation Strategies*, 2025, DOI: 10.5772/intechopen.1011788.
28 Y. Fan, J. Ren, Y. Cao, Y. Zou, X. Xiao and F. Liu, *Compr. Rev. Food Sci. Food Saf.*, 2025, **24**(6), e70334.
29 R. P. Popa and A. F. Tabaran, *Appl. Sci.*, 2025, **15**, 6135.
30 S. Pregent, C. L. Hoad, E. Ciampi, M. Kirkland, E. F. Cox, L. Marciani, R. C. Spiller, M. F. Butler, P. Gowland and P. Rayment, *Food Hydrocoll.*, 2012, **26**, 187–196.
31 D. Liu and M. Shimizu, Ingesting chitosan can promote-excretion of microplastics, *Sci. Rep.*, 2025, **15**(1), 14041.